IEEE *Access*
Multidisciplinary : Rapid Review : Open Access Journal

Enhanced-Performance Circularly Polarized MIMO Antenna with Polarization/Pattern Diversity

Ubaid Ullah[1], Ismail Ben Mabrouk[1], Senior Member, IEEE and Slawomir Koziel[2], Senior Member, IEEE

[1]Networks and Communication Engineering department, Al Ain University, P.O.Box (112612), Abu Dhabi, UAE
[2]Engineering Optimization and Modeling Center of Reykjavik University, Reykjavik, Iceland

Corresponding author: U. Ullah (e-mail: ubaid.ullah@aau.ac.ae).

ABSTRACT Design of a compact wideband circularly polarized (CP) multiple-input multiple-output (MIMO) antenna with polarization diversity is proposed and characterized for off-body communication. The antenna is based on a simple coplanar waveguide (CPW)-fed monopole extension of the microstrip line. The orthogonal field components required by CP are induced using a simply modified right/left side ground plane. In particular, a stub extending from the ground plane along the length of the microstrip line generates the vertical component, whereas the current along the width of the ground plane contributes to the horizontal components. To obtain a unidirectional radiation pattern in the off-body direction and to reduce the sensitivity to the human body loading effects, a flat reflector printed on a high permittivity flexible substrate is applied. The simple topology of the antenna can be described by a few adjustable parameters, which facilitates its EM design closure. Prior to the experimental validation in the free space and on the body, the antenna is optimized at the full-wave level of description for all major performance figures. The overall footprint of the antenna radiator is only $L_s \times W_s = 0.24\ \lambda_0 \times 0.64\ \lambda_0 = 0.15\ \lambda_0^2$. The proposed MIMO antenna features $|S_{11}| \leq$ -10 dB, average isolation $|S_{21}| \leq$ -22 dB, and axial ratio (AR) $\leq$ 3 dB from 5.2 GHz to 6.3 GHz with 100% bandwidth overlap between the impedance and axial ratio bandwidths. The envelope correlation coefficient (ECC) is less than 0.004 with the maximum diversity gain (DG) of approximately 9.99 dB. Moreover, the antenna maintains a high efficiency of up to 90% when loaded on the body, and a low specific absorption rate (SAR).

INDEX TERMS Circular polarization antennas, MIMO antennas, compact antennas, wideband antennas, simulation-driven design.

I. INTRODUCTION

This to the multiple-input multiple-output (MIMO) technology, the performance of wireless communication systems has been significantly improved over recent years [1], [2]. The MIMO technology has been standardized and currently it is an essential part of the consumer electronics operating within the 2.4 GHz and 5.8 GHz WiFi, WiMax, 4G and LTE technologies. The MIMO technology utilizes the multipath propagation concept by employing multiple antennas to transmit and receive more than one signal simultaneously over the same radio channel. In comparison to the single-input single-output (SISO) standard, MIMO systems allow for high capacity, improved spectral efficiency and highly reliable communication link between the transmitter and the receiver [2], [3].

To further enhance the performance of the MIMO systems, it is important to minimize co-channel interference and multipath fading. It is well known that highly isolated antennas can improve the performance of the system by reducing coupling between the antennas [3]. A variety of isolation techniques have been adopted to ensure the independent operation of the antenna in MIMO communication. The most commonly used decoupling technique is to place the two antennas orthogonally. However, this technique adds to the complexity of the feeding circuit [4-6]. In addition, the integration of electromagnetic bandgap (EBG) structures, adding parasitic elements and/or implementing neutralization lines could also improve the isolation between the MIMO antennas [3]. Nevertheless, when using these approaches, additional elements are added which increases the overall

footprint of the antenna [7]. On the other hand, polarization and pattern diversities are promising techniques to reduce the correlation between the antenna far-fields without increasing the size of the circuit [8-9]. In [10-11], it has been shown that the performance of the MIMO system in terms of channel capacity and diversity gain (DG) can be dramatically improved when both the polarization and pattern diversities are incorporated.

Modern portable communication devices, especially those used for wearable applications, require the system to be compact, low profile, lightweight, low cost and highly efficient [12-17]. When the antenna is worn on the human body, it is exposed to a large volume of lossy material in its immediate vicinity. This degrades the performance by converting the near electric field of the antenna into the heat energy [18],[19]. Moreover, the polarization mismatch losses further degrade the antenna performance in body-centric applications, especially when linearly polarized (LP) antennas are involved. On the other hand, circular polarization (CP) antennas have the advantage of reduced signal attenuation, multipath fading, and absorption losses [20-23]. Furthermore, signal transmission/reception is independent of the orientation/positioning of the CP antenna [24]. Due to these characteristics, CP antennas have been widely used in the currently available technologies and are to be applied in the emerging ones. As of now, most of the antennas proposed in the literature for wearable applications are LP; they are prone to detuning and may lead to unreliable data communication [25-29]. To date, limited work has been done on CP antennas for body-centric applications, especially in the 5 GHz band. It appears that a reasonable approach to meet the challenges associated with wearable antennas is the design of a multiple antenna system with circular polarization and polarization diversity.

In this paper, a compact and geometrically simple circularly polarized MIMO antenna with polarization diversity is presented. A single-element antenna is first designed with the right-hand circular polarization (RHCP). The antenna comprises a simple coplanar waveguide (CPW)-fed monopole extension of the microstrip line and a modified coplanar ground plane. The vertical component of the CP is induced through a protruded stub in the right-side ground plane; the horizontal components are excited along the width of the left-side ground plane. Having in mind wearable off-body communication and reduction of the loading effects, a high permittivity reflector is placed a quarter wavelength away from the antenna. The proposed topology allows for easy mirroring of the structure and hence its sense of polarization. The MIMO antenna is implemented in a parallel configuration with polarization diversity achieved by switching the positions of the coplanar ground planes. The pattern diversity is realized by mechanically bending the backside flexible reflector. The geometrical simplicity of the structure can be described by a few parameters, which facilitates its electromagnetic (EM) design closure. All parameters are optimized at the full-wave

level of description. The total footprint of the MIMO antenna is only (13.7 mm × 36.2 mm) 0.15 λ_0^2 at the lowest operating frequency.

The antenna prototype is fabricated and the numerical results are validated experimentally in the free space and on the body. The antenna features excellent impedance matching and axial ratio from 5.2 GHz to 6.3 GHz in both free space and on-body with average isolation $|S_{21}| \leq -20$ dB. The envelope correlation coefficient (ECC) is less than 0.004 with the maximum DG of approximately 10 dB. The average total efficiency of the antenna is 90% when worn on the body with the specific absorption rate (SAR) of 0.133 W/ Kg and 0.058 W/kg for 1 g and 10 g of human tissue respectively. The antenna can be effectively used for ISM bands in 5 GHz range and Unlicensed National Information Infrastructure (U-NII). The contributions of this work include: (i) design of a new unidirectional CP MIMO antenna with polarization/pattern diversity covering U-NII worldwide band and ISM 5.8 GHz band; (ii) obtaining reduced loading effects of the human body owing to the unidirectional topology and high permittivity substrate used as a reflector; (iii) demonstrably improved overall performance as compared to the range of comparable CP state-of-the-art structures reported in the literature.

II. ANTENNA DESIGN AND ANALYSIS

A. SINGLE ELEMENT DESIGN

The parameterized front and side views of the single element design are shown in Figs. 1(a) and 1(b), respectively. Figure 1(c) shows the MIMO configuration. The antenna structure is implemented on a rigid laminated Rogers substrate RO4003C ($\varepsilon_r = 3.38$, $\tan\delta = 0.0027$, thickness $h = 0.813$) with external dimensions $L_s \times W_s = 13.7 \times 13.2 = 0.24 \lambda_0 \times 0.23 \lambda_0$. The front side of the radiating element consists of a 50-ohm CPW feed and a quarter wavelength long microstrip line extension.

The initial single element antenna is designed for RHCP by protruding a stub from the right-side ground plane along the length L_m of the microstrip line. The vertical electric field component E_v is induced through the stub of the length L_1 extending from the right-side ground plane along the y-direction. The orthogonal component E_H is excited by the current along the x-direction on the left-side ground plane. The stub extension generates the orthogonal components for CP and also improves the impedance matching by lengthening the current path within the ground plane.

The CP mechanism of the antenna will be further explained in the next section using the surface current distribution. At the bottom of the antenna, a large size flat reflector implemented using a flexible high permittivity substrate Rogers RT3010 ($\varepsilon_r = 10.2$, $\tan\delta = 0.0027$, thickness $h = 0.635$) is placed a quarter wavelength away from the antenna. The reflector serves two purposes: it directs the radiated power in the off-body direction and reduces the performance-degrading effects of the human body.
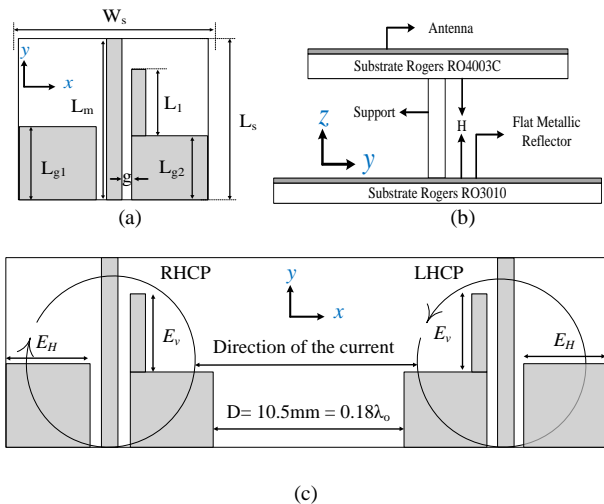
FIGURE 1. Geometry of the proposed CP antenna (all parameter values in mm): (a) top view (b) side view. L_1= 6.39, L_{g1}=6.1, L_{g2}=5.39, L_m=13.74, g=0.6325, L_s=13.77, H=13.626 and W_s= 12.99 (c) MIMO configuration.

Moreover, the flexibility of the reflector substrate makes it easy to bend and adjust to the human body curvatures. The computational model of the antenna is implemented in CST Microwave Studio and the adjustable parameters are optimized at the full-wave EM level of description. For reliable experimental characterization and validation of the antenna, the model incorporates the SMA connector.

B. MIMO DESIGN AND CP MECHANISM

The MIMO antenna system is implemented with polarization diversity, according to the configuration shown in Fig. 1(c). The total area of the antenna is only 13.7 mm × 36.2 mm.

The two antennas are positioned in parallel with the distance D = 10.5 mm, equivalent to $0.18\lambda_0$ at the lowest operating frequency of the antenna. To achieve RHCP and LHCP, the right-side and left-side ground planes of the CPW are extended in the y-direction respectively. The inverse correlation of the two antennas is shown by highlighting the direction of the current on the surface of the antennas.

In order to induce circular polarization, simultaneous excitation of two orthogonal field components with equal amplitude is needed. To explain the CP operation of the proposed antenna, the surface current distribution is shown in Fig. 2 for one sense of polarization at the center frequency. Note that the surface current distribution is calculated from the magnetic field vectors. As seen from the surface current distribution, two orthogonal components are generated in the conducting coplanar ground planes. The direction of the arrows indicates the orientations of the dominant field components at different angular time intervals. At zero degrees, the current is predominantly located in the +y-direction along the length of the stub extension from the right-side ground plane which corresponds to the E_v. At 90-degrees, the field position changes to +x-direction and the dominant field components are located along the width of the left-side ground plane contributing to the horizontal E_H component. Similarly, at 180-degrees and 270-degrees, the direction of the current changes to –y-direction and –x-direction respectively.

As it can be observed from the current path, the electric field vector field is rotating in the clockwise direction, therefore, the sense of polarization of this topology is RHCP. The proposed antenna structure can be easily re-designed for LHCP by simply switching the positions of the coplanar ground planes. The total footprint of the single element is only $0.05\lambda_0^2$, with the maximum linear dimension of 13.74 mm. According to the formula of the far-field region $2D^2/\lambda$, the two antennas are placed in the far-field region where the electromagnetic fields are dominated by the radiating fields, therefore, spatial diversity comes into effect. This improves the antenna isolation. Note that generally, the minimum distance between the two antennas is 0.5λ, but due to the small size of the proposed structure, excellent isolation has been achieved with only 0.18λ. Additionally, there is no physical ground plane or metallization connecting both the antenna elements and also the inherent characteristics of polarization and pattern diversities add to the improvement of isolation [33] [34]. To clarify this further, surface current distributions are illustrated in Fig. 2(e) when port 1 is excited and Fig. 2 (b) when port 2 is excited.
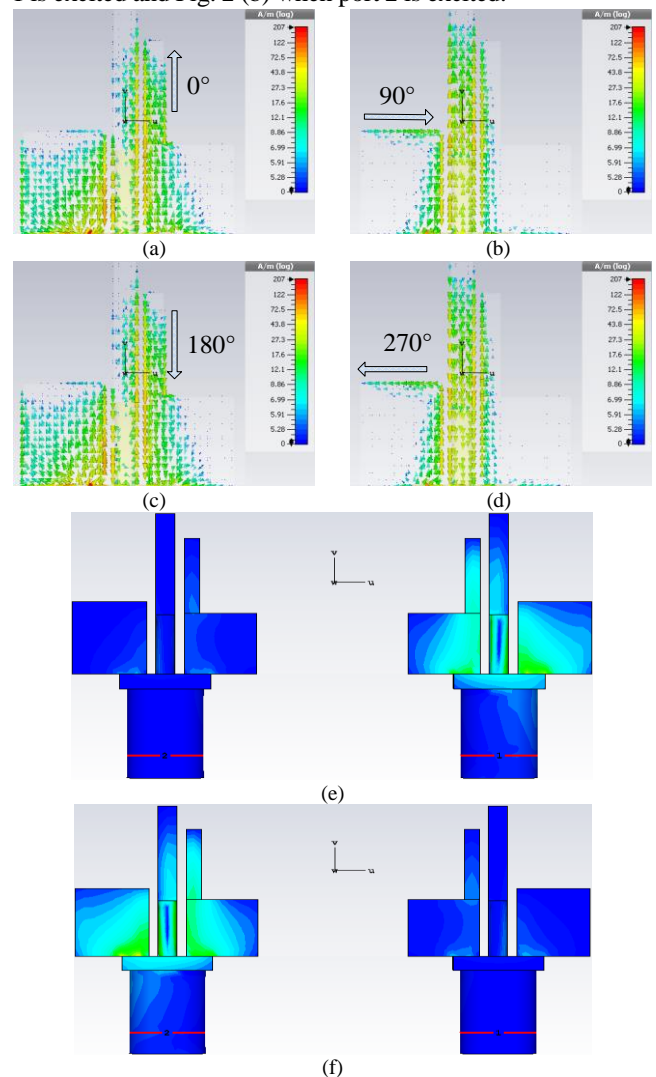

FIGURE 2. Circular polarization mechanism of the proposed antenna. Current distributions at 5.6 GHz for (a) 0-degrees (b) 90-degrees (c) 180-degrees (d) 270-degrees (e) Surface current Port 1 (f) Surface current Port 2

C. PARAMETER TUNING

All antenna parameters are optimized at the full-wave level of description. This is necessary in order to improve the performance as much as possible, while handling all relevant antenna characteristics, including the reflection response, element isolation, and axial ratio. Due to the simple topology, the structure is described using only a few variables, denoted as $x = [L_1\,L_{g1}\,L_{g2}\,L_m\,L_s\,W_1\,W_{g1}\,W_{g2}]^T$.

Here, W_1 corresponds to the width of the extended stub, W_{g1} and W_{g2} are the widths of the left-side and right-side ground planes respectively. The width W_s of the antenna is dependent on W_{g1}, and W_{g2}. To ensure the maximum in-band reflection remains below – 10 dB and AR below 3 dB, a multi-stage optimization procedure is adopted. The optimization task is formulated as

$$x^* = \arg\min_{x} U\left(BW_S(x), S(x), AR(x)\right) \quad (1)$$

where U is the objective function, $BW_S(x)$ is the symmetric – 10 dB bandwidth around 5.5 GHz, $S(x)$ is the maximum in-band reflection for the bandwidth of interest (here, the range covering the U-NII and ISM 5 GHz bands), whereas $AR(x)$ is the maximum in-band axial ratio (within the same bandwidth of interest).

Two separate sub-problems are considered. At the first stage, the goal is to maximize BW_S in order to obtain a good initial design for the next optimization stage. Here, the objective function is defined as

$$U_S\left(BW_S(x), S(x), AR(x)\right) = -BW_s(x) + \beta_S c_S(S(x))^2 \quad (2)$$

where $c_S(S(x)) = \max\{(S(x) + 10, 0\}/10$ is a penalty function that "measures" a relative violation of the condition $S(x) \leq -10$ dB, and β_S is a penalty factor. The second task is to minimize $AR(x)$, for which the cost function is defined as

$$U_{AR}\left(BW_S(x), S(x), AR(x)\right) = AR(x) + \beta_S c_S(S(x))^2 \quad (3)$$

which allows for reducing the in-band axial ratio while retaining the acceptable level of antenna reflection.

Both sub-problems are solved using a trust-region gradient search with numerical derivatives [35]. The algorithm yields a series $x^{(i)}$, $i = 0, 1, \ldots,$ of approximations to the optimum design x^* of (1), generated as

$$x^{(i+1)} = \arg\min_{x;\, -d^{(i)} \leq x - x^{(i)} \leq d^{(i)}} U(L^{(i)}(x)) \quad (4)$$

where

$$L^{(i)}(x) = R(x^{(i)}) + J_R(x^{(i)}) \cdot (x - x^{(i)}) \quad (5)$$

In (5), R stands for the aggregated antenna outputs, here, evaluated using the time-domain solver of CST Microwave Studio, whereas J_R is the Jacobian matrix estimated using finite differentiation. The search process in (5) is restricted to the vicinity of the current design, determined by the trust

region size vector $d^{(i)}$, so that $x^{(i)} - d^{(i)} \leq x \leq x^{(i)} + d^{(i)}$. The inequality is understood component-wise. The trust region size is adjusted adaptively (cf. [35]).

Figure 3 shows the antenna characteristics at the initial and the optimized design. Notice that the isolation $|S_{12}|$ can be further improved by simply increasing the separation D between the antennas, which, however, leads to an increase of the system size. The final optimized values corresponding the vector x are $x^{(0)} = [6.39\ 6.18\ 5.39\ 13.74\ 13.77\ 1.05\ 5.04\ 5.18]^T$.

III. NUMERICAL RESULTS AND EXPERIMENTAL VALIDATION

A. S-PARAMETERS AND AXIAL RATIO

The proposed MIMO antenna has been fabricated and characterized in the free space and on the body of a human volunteer (22 years of age, weight 83 kg, height 180 cm). The prototype and the on-body experimental setup (arm and chest) are shown in Fig. 4. The experimental characterization of the antenna has been carried out in the anechoic chamber of Reykjavik University, Iceland.

The measurement was performed on Port 1 while Port 2 was terminated with a 50-ohm load. The simulated and measured S_{11} of the antenna are shown in Figs. 5. The reflection response shows that the antenna provides the impedance bandwidth ($|S_{11}| \geq$ -10 dB) from 5.2 GHz to 6.3 GHz. It can be observed that the on-body measured S_{11} of the antenna shows certain improvement, i.e., reduced mismatch losses. This is due to the presence of the human body which absorbs some of the input energy. The S_{21} response illustrated in Fig. 6 shows that the average isolation is better than –20 dB within the antenna operating bandwidth.

The AR responses of the antenna in the broadside direction are depicted in Fig. 7. The axial ratio of the antenna is measured using the polarization-pattern method. The simulation and measurement result in the free space shows that the antenna maintains AR below 3 dB in the antenna operating bandwidth with 100% bandwidth overlap between S_{11} and AR.
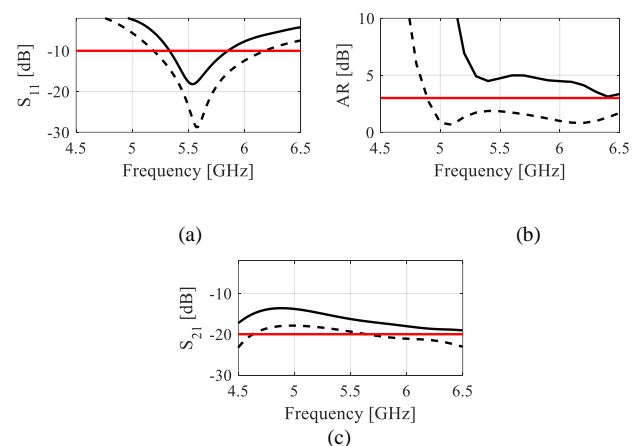

FIGURE 3. Antenna optimization: initial design (—), and optimized design (- - -). (a) $|S_{11}|$, (b) AR (c) $|S_{21}|$
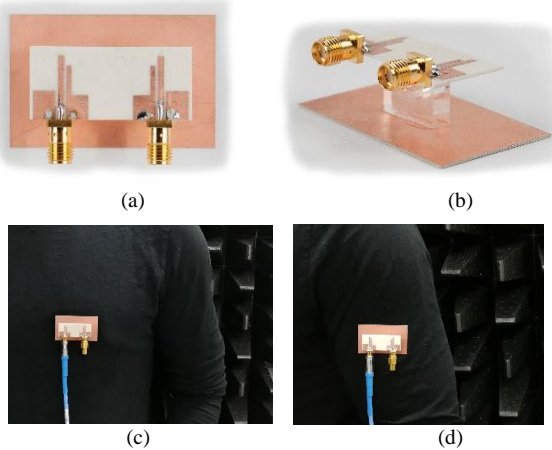
FIGURE 4.. Antenna prototype and characterization setup: (a) Front view, (b) Perspective view (c) on chest characterization (d) on arm characterization.
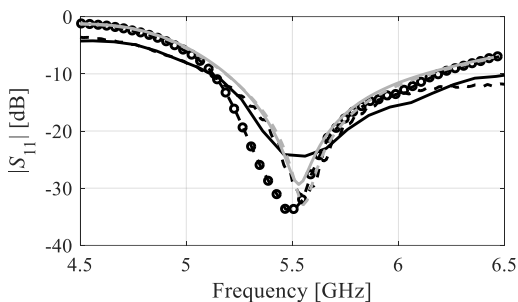

FIGURE 5. Simulation (gray) and measured (black) antenna $|S_{11}|$ characterization, free-space (—), on-arm (- - -), and on chest (- o -).
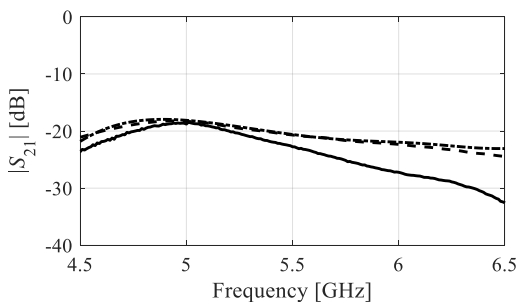

FIGURE 6. Simulation and measured S_{21}. Simulation free-space (- . -), simulation on-arm (- - -), and measured (—).
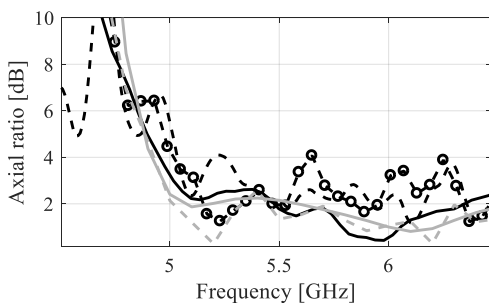

FIGURE 7. Simulation (gray) and measured (black) antenna AR characterization. free-space (—), on-arm (- - -), and on chest (- o -).

The on-body measurement, especially on the chest, shows a slight deviation of AR from the 3 dB requirement at certain frequency points. The reason for this deviation could be the

foreseeable slight movements of the volunteer during the measurement process.

B. REALIZED GAIN AND EFFICIENCY

The simulated and measured realized gain of the antenna is illustrated in Fig. 8. The peak gain of the antenna is approximately 5.8 dBic with a discrepancy of 1.7 dB between the free-space and on body measurements. When the antenna is loaded on the chest it is surrounded by the lossy material in all directions which results in a degradation of the gain, especially in the upper frequency band. Another important performance figure of the antenna is the efficiency which has been shown in Fig. 9. The simulated and measured radiation efficiency of the antenna in free space is more than 95% in the entire operating band, while it drops to approximately 90% when simulated on-body. Moreover, the total efficiency of the antenna also shows similar trend for both free space and on-body analysis. Unlike the traditional textile based antenna (with low conductivity), the proposed antenna retains high efficiency in the presence of the human body and no significant overall performance degradation.

C. RADIATION PATTERN

The antenna radiation pattern is characterized in the *xz*- and the *yz*-planes as shown in Fig. 10. As mentioned before, the antenna is characterized for one port, therefore only one sense of polarization is considered, which is RHCP in this case. The normalized RHCP and LHCP patterns are shown at three different frequency points for both simulation and measurements.
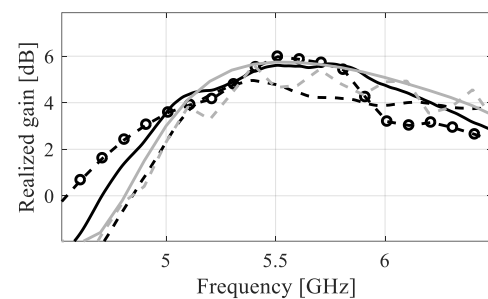

FIGURE 8. Simulation (gray) and measured (black) antenna AR characterization. free-space (—), on-chest (- - -), and on-arm (- o -).
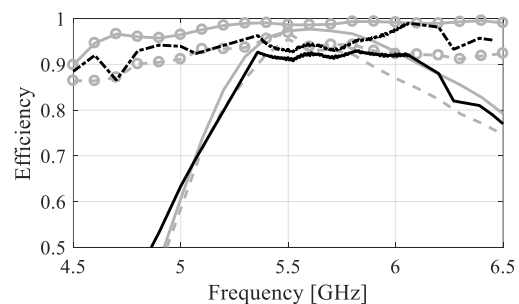

FIGURE 9. Simulation (gray) and measured (black) antenna efficiencies. Total efficiency free-space (—), total efficiency on-body (- - -), radiation efficiency (o—o), radiation efficiency on body (- o -), and radiation efficiency free-space (- . -).
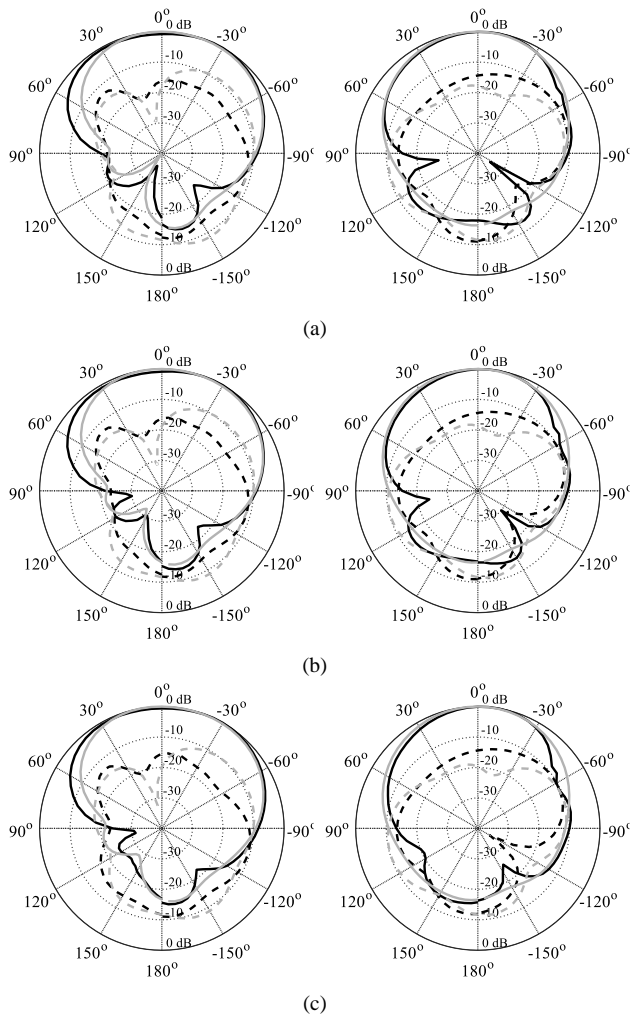
FIGURE 10. The normalized radiation pattern of the proposed MIMO antenna in the *xz*-plane (left-hand-side panel) and the *yz*-plane (right-hand-side panel) (a) 5.5 GHz, (b) 5.6 GHz, and (c) 5.7 GHz.

The difference between the RHCP and LHCP in the broadside direction is more than 17 dB for both planes and the antenna maintains a steady radiation pattern in the +z-direction.

D. BENDING EFFECTS ON S-PARAMETER AND AR

When the antenna is worn on the human body, the person may change the posture resulting in a certain amount of structural deformation. Therefore, for body-worn applications, the antenna needs to retain acceptable performance when bended to some extent. It should be noticed that a flat reflector behind the antenna is implemented using a high permittivity substrate which is flexible.

To evaluate the antenna conformability to the human body, the antenna is tested for different curvature radii ($r = 15$ mm, and 35 mm) and the major performance figures are analyzed. It is important to mention here that the direction of the excitation line and the surface current orientation is mostly along the *y*-direction (cf. Fig. 2). To avoid frequency detuning, the ground plane reflector is bended only in the *x*-direction which also happens to be the largest dimension of the antenna. The

reflection response indicates that bending has an almost negligible effect on the antenna impedance bandwidth, but the impedance matching is deteriorated by roughly 6 dB. Still, the antenna impedance matching is well below –10 dB acceptance level throughout the operating band as illustrated in Fig. 11. The axial ratio characteristics exhibit similar behavior. In particular, AR below 3 dB is maintained for 100 percent of the impedance bandwidth. The S_{12} characteristic is also shown in Fig. 11(a), which indicates that the isolation of between the two elements is not affected with the reflector deformation. Clearly, stable S_{21} follows from the fact that that bending of the reflector does affect the physical separation between the two parallel ports. However, compared to the results without reflector deformation (cf. Fig. 6), the isolation has improved by roughly 2 dB which is attributed to the inherent characteristics of pattern diversity.

E. PATTERN DIVERSITY

Pattern diversity can significantly enhance the performance of the MIMO system. Along with the polarization diversity, the proposed design has the advantage of achieving pattern diversity by mechanically bending the reflector. As mentioned in the preceding section, the antenna maintains excellent impedance bandwidth and AR characteristics when the backside reflector is bended to a certain degree.

Another noteworthy effect of bending the reflector is the diversification of the radiation pattern. Figure 12 shows the simulated radiation pattern of the antenna at the center frequency with different bending curvature radii of 15 mm, and 35mm. The analysis was performed for several bending radii (15 mm, 20 mm, 25 mm and 35 mm) but only two values are shown for brevity. As it can be clearly observed from the patterns, the main beam direction of the antenna changes from $\theta = 0$ degrees to $\theta = 60$ degrees with the progressive decrease in the bending radii.
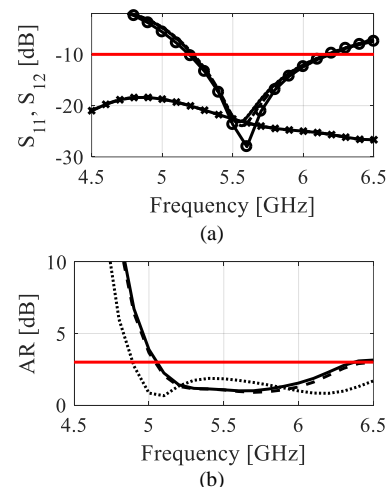

FIGURE 11. Bending effects on the antenna characteristics (a) $|S_{11}|$, $r = 0$ mm bend (o—o), $r =15$ mm bend (—), and $r = 35$ mm bend (---), and $|S_{12}|$, $r =15$ mm bend (—), and $r = 35$ mm bend (-x-), (b) AR, $r = 0$ mm bend (....), $r = 15$ mm bend (—), and $r = 35$ mm bend (---).

The effective pattern diversity between the two antennas of 120-degree is easily achieved without serious degradation of other performance figures of the antenna. The pattern diversity of the antenna can be realized when the antenna is in bent condition, in particular when worn on wrist, arm or ankle.

F. ENVELOPE CORRELATION COEFFICIENT AND DIVERSITY GAIN

One of the major figures of the MIMO system is ECC, which quantifies the diversity performance of the antenna. ECC can be calculated from the scattering parameters or from the far-field radiation pattern. For high-efficiency antennas, the *S*-parameter-based calculation is generally valid [25]. Therefore, in this paper, we show the simulated and measured ECC obtained this way, i.e.,

$$\rho e, ij \ = \ \frac{|\iint_{4\pi}[\vec{F_i}(\theta,\phi)*\vec{F_j}(\theta,\phi)]d\Omega|^2}{\iint_{4\pi}|\vec{F_i}(\theta,\phi)|^2*\iint_{4\pi}\vec{F_j}(\theta,\phi)|^2} \quad (4)$$

as well as the simulated ECC determined from the radiation pattern. Another important characteristic is DG which is calculated as

$$DG = 10\sqrt{1 - |0.99\rho e|^2} \quad (5)$$

The corresponding results are depicted in Fig. 13 and Fig. 14. It can be seen that the ECC of the proposed antenna is below 0.002 which indicates high diversity up to 9.99 dB.

G. SAR EVALUATION

The SAR of the antenna is evaluated for 1 g and 10 g of the human tissue based on the on-body simulation. The permittivity, conductivity, blood flow and other biological characteristics of the human phantom are set according to the CST Microwave Studio voxel data. SAR is a factor that measures the amount of energy absorbed by the per-unit mass of the human tissue. To compare the performance of the proposed antenna, the safety standard of 1.56 W/kg and 1.96 W/kg are used as benchmarks. The SAR evaluation on the body is shown in Fig. 15. The result indicates that the

maximum SAR for 1g and 10 g of human tissue is 0.134 W/kg and 0.058 W/kg respectively which is well below safety limits defined by the United States and Europe.
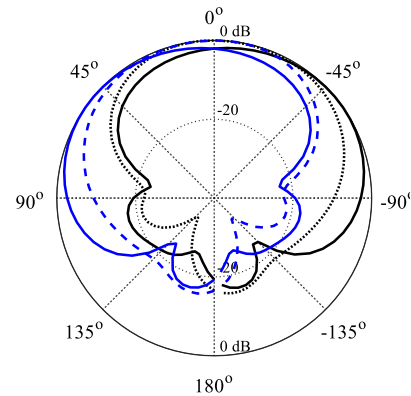

FIGURE 12. LHCP (blue) and RHCP (black) radiation pattern diversity of the antenna for chosen radii, *r* = 15 mm (—), and *r* = 35 mm (- - -).
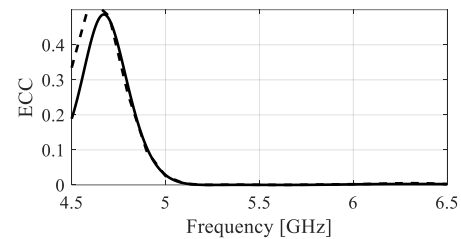

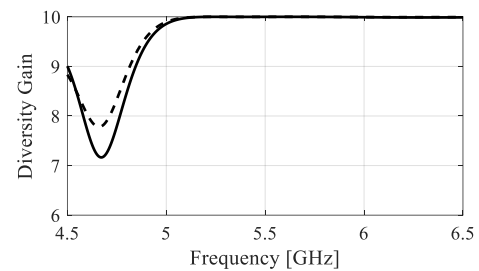**FIGURE 13.** Envelop Correlation Coefficient. Simulated (—), and calculated (- - -)

FIGURE 14. Simulated (—) and calculated (- - -) diversity gain.

TABLE I COMPARISON WITH STATE-OF-THE-ART MIMO ANTENNAS

Reference	Operating frequency (GHz)	Diversity	Polarization	Size [λ_o^2]	Isolation (dB)	On Body Analysis	Gain (Free Space) (dBi)	Gain (On-body) (dBi)	%AR	%BW
[4]	5.5	Polarization / Pattern	Circular	0.25	13	No	~ 4.5	----	4.7	----
[5]	5.3	Polarization / Pattern	Linear/Circular	0.43	18	No	2.85	----	2.32	16.28
[30]	3.3	Polarization /Spatial	Linear	0.61	25	No	4	----	----	28.5
[31]	2.4	Polarization / Pattern	Dual	0.09	12	Yes	2.79	1.67	----	20
[32]	2.4/5.15	---	Linear	0.26	15	No	----	----	----	8.2
Proposed	5.2	Polarization / Pattern	Circular	0.16	22	Yes	5.8	4.1	18.3	18.3

H. BENCHMARKING

The proposed design has been compared with state-of-the-art antennas from the literature in terms of the type of diversity employed, polarization, radiator size, isolation, free-space analysis, on-body analysis, axial ratio, and impedance bandwidth are compared. It should be emphasized that the literature is sparse concerning MIMO antennas for wearable applications, therefore the comparison table (Table I) contains the designs that might only partially overlap with the proposed one in terms of the operating conditions and the performance figures. For fair comparison, the antenna operating frequencies are also included in the table; the antenna sizes are calculated for the lowest free-space operating frequency. As it can be observed from the table, the proposed antenna is competitive with respect to almost all considered figures.

In particular, compared to the antennas of [4] and [5] employing the same types of diversity and implementing circular polarization, our design offers a significantly smaller size, better isolation, higher gain, and considerably wider axial ratio bandwidth. It is also worth noticing that unlike in [4] and [5], the AR bandwidth is consistent with the impedance bandwidth which emphasizes a proper parameter tuning (cf. Section II.C) as a keystone for boosting the antenna performance with respect to all relevant figures of interest. Furthermore, the proposed antenna demonstrably exhibits excellent on-body characteristics, including relatively high gain (not reported for the benchmark cases). The remaining competitive structures, [30]-[32], are also shown inferior despite being designed for linear polarization only.

IV. CONCLUSION

In the paper, a simple topology, circularly polarized MIMO antenna with polarization and pattern diversity is presented and validated for wearable applications. The single-element design of the proposed antenna comprises a CPW-fed monopole radiator and a modified ground plan for achieving one sense of circular polarization. For implementing the MIMO design, two antennas are allocated in parallel, and the positions of the coplanar ground planes are mirrored to achieve polarization diversity.
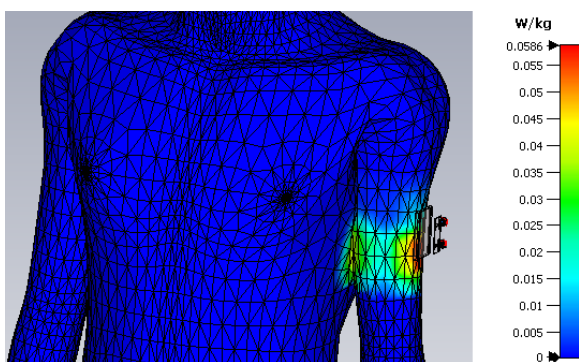
The antenna is tested for body-worn application with different bending curvature radii which further improves the performance of the antenna by introducing the pattern diversity in the antenna. The simple geometry of the antenna is only described by a few adjustable parameters, which were fully optimized at the full-wave level of description. The total foot-print of the antenna radiator is only $0.24\lambda_0 \times 0.64\lambda_0 = 0.15\lambda_0^2$. The proposed design maintains stable performance in both free-space and in body-worn scenario. The antenna impedance bandwidth and AR bandwidth is 18%, isolation $|S_{21}| \leq$ - 22 dB, efficiency ~ 90% (on body), ECC < 0.04, and SAR 0.134 W/kg for 1 gram of human tissue. The proposed antenna is suitable for a number of applications including wearable applications in U-NII band and ISM 5.8 GHz band. Compared to the single-layer designs, multi-layer structures are not convenient to implement, but they effectively improve the performance of the antenna in the proximity of the human body.

REFERENCES

[1] F. A. Dicandia, S. Genovesi, and A. Monorchio, "Analysis of the performance enhancement of MIMO systems employing circular polarization," *IEEE Trans. Antennas Propag.,* vol. 65, no. 9, pp. 4824-4835, Sept. 2017.

[2] M. A. Jensen and J. W. Wallace, "A review of antennas and propagation for MIMO wireless communications," *IEEE Trans. Antennas Propag.,* vol. 52, no. 11, pp. 2810–2824, Nov. 2004.

[3] M. A. Ul Haq and S. Koziel, "Ground plane alterations for design of high-isolation compact wideband MIMO antenna," *IEEE Access*, vol. 6, pp. 48978-48983, 2018.

[4] J. Malik, A. Patnaik, and M. V. Kartikeyan, "Novel printed MIMO antenna with pattern and polarization diversity," *IEEE Antennas Wireless Propag. Lett.,vol.* 14, pp. 739-742, 2015.

[5] Y. Sharma, D. Sarkar, K. Saurav, and K. V. Srivastava, "Three-element MIMO antenna system with pattern and polarization diversity for WLAN applications," *IEEE Antennas Wireless Propag. Lett.,* vol. 16, pp. 1163-1166, 2017.

[6] I. Ahamed and M. Vijay, "Comparison of different diversity techniques in MIMO antennas," *2nd International Conference on Communication and Electronics Systems (ICCES)*, Coimbatore, pp. 47-50, 2017.

[7] S. M. Mikki and Y. M. M. Antar, "On cross correlation in antenna arrays with applications to spatial diversity and MIMO systems," *IEEE Trans. Antennas Propag.,* vol. 63, no. 4, pp. 1798-1810, April 2015.

[8] P. Qin, Y. J. Guo, and C. Liang, "Effect of antenna polarization diversity on mimo system capacity," *IEEE Antennas Wireless Propag. Lett.,* vol. 9, pp. 1092-1095, 2010.

[9] L. C. Chang, C. H. Tsai, P. Hsu, and C. C. Liu, "A polarization diversity MIMO antenna design for WiMAX dongle application," *Proc. Asia-Pacific Microw. Conf.,* pp. 762-765, 2010.

[10] J. Zhu, S. Li, B. Feng, L. Deng, and S. Yin, "Compact dual polarized UWB quasi-self-complementary MIMO/diversity antenna with band-rejection capability," *IEEE Antennas Wireless Propag. Lett.,* vol. 15, pp. 905–908, 2016.

FIGURE 15. SAR analysis on the human arm for 10 grams of tissue.

This article has been accepted for publication in a future issue of this journal, but has not been fully edited. Content may change prior to final publication. Citation information: DOI 10.1109/ACCESS.2020.2966052, IEEE Access

IEEE *Access*
Multidisciplinary : Rapid Review : Open Access Journal

[11] D. Sipal, M. P. Abegaonkar, and S. K. Koul, "Highly isolated compact planar dual-band antenna with polarization/pattern diversity characteristics for MIMO terminals," *IEEE Antennas Wireless Propag. Lett.,* vol. 18, no. 4, pp. 762-766, April 2019.

[12] A. Boukarkar, X. Q. Lin, Y. Jiang, L. Y. Nie, P. Mei, and Y. Q. Yu, "A miniaturized extremely close-spaced four-element dual-band MIMO antenna system with polarization and pattern diversity," *IEEE Antennas Wireless Propag. Lett.,* vol. 17, no. 1, pp. 134-137, Jan. 2018.

[13] K. N. Paracha, S.K. A. Rahim, P.J. Soh, M.R. Kamarudin, K.G. Tan, Y.C. Lo, and M.R. Islam, "A low profile, dual-band, dual polarized antenna for indoor/outdoor wearable application," *IEEE Access.,* vol. 7, pp. 33277-33288, 2019.

[14] X. Y. Liu, Z. T. Wu, Y. Fan, and E. M. Tentzeris, "A miniaturized CSRR loaded wide-beamwidth circularly polarized implantable antenna for subcutaneous real-time glucose monitoring," *IEEE Antennas Wireless Propag. Lett.,* vol. 16, pp. 577–580, 2017.

[15] Z. H. Jiang, Z. Cui, T. Yue, Y. Zhu, and D. H. Werner, "Compact, highly efficient, and fully flexible circularly polarized antenna enabled by silver nanowires for wireless body-area networks," *IEEE Trans. Biomed. Circuits Syst.,* vol. 11, no. 4, pp. 920–932, Aug. 2017.

[16] X.-Q. Zhu, Y.-X. Guo, and W. Wu, "Miniaturized dual-band and dual-polarized antenna for MBAN applications," *IEEE Trans. Antennas Propag.,* vol. 64, no. 7, pp. 2805–2814, Jul. 2016.

[17] H. Xiaomu, S. Yan and G. A. E. Vandenbosch, "Wearable Button Antenna for Dual-Band WLAN Applications With Combined on and off-Body Radiation Patterns," IEEE Transactions on Antennas and Propagation, vol. 65, no. 3, pp. 1384-1387, March 2017.

[18] B. S. Abirami and E. F. Sundarsingh, "EBG-backed flexible printed Yagi–Uda antenna for on-body communication," *IEEE Trans. Antennas Propag.,* vol. 65, no. 7, pp. 3762–3765, Jul. 2017.

[19] X. Hu, S. Yan, and G. A. E. Vandenbosch, "Compact circularly polarized wearable button antenna with broadside pattern for U-NII worldwide band applications," *IEEE Trans. Antennas Propag.,* vol. 67, no. 2, pp. 1341-1345, Feb. 2019.

[20] U. Ullah and S. Koziel, "A novel coplanar-strip-based excitation technique for design of broadband circularly polarization antennas with wide 3 db axial ratio beamwidth," *IEEE Trans. Antennas Propag.,* vol. 67, no. 6, pp. 4224-4229, June 2019.

[21] U. Ullah and S. Koziel, "A geometrically simple compact wideband circularly polarized antenna," *IEEE Antennas Wireless Propag. Lett.,* vol. 18, no. 6, pp. 1179-1183, June 2019.

[22] J. K. Pakkathillam and M. Kanagasabai, "Circularly polarized broadband antenna deploying fractal slot geometry," *IEEE Antennas Wireless Propag. Lett.,* vol. 14, pp. 1286-1289, 2015.

[23] M.F. Ain, U. Ullah, and Z.A. Ahmad. "Bi-Polarized dual-segment rectangular dielectric resonator antenna," *IETE Journal of Res*., vol.59, pp.739-743, 2013.

[24] U. Ullah and S. Koziel, "A broadband circularly polarized wide-slot antenna with a miniaturized footprint," *IEEE Antennas and Wireless Propag Lett.,* vol. 17, no. 12, pp. 2454-2458, Dec. 2018.

[25] Z. H. Jiang and D. H. Werner, "A compact, wideband circularly polarized co-designed filtering antenna and its application for wearable devices with low SAR," *IEEE Trans. Ant. Propag.,* vol. 63, no. 9, pp. 3808-3818, Sept. 2015.

[26] Z. H. Jiang, Z. Cui, T. Yue, Y. Zhu, and D. H. Werner, "Compact, highly efficient, and fully flexible circularly polarized antenna enabled by silver nanowires for wireless body-area networks," *IEEE Trans. Biomedical Circuits Syst.,* vol. 11, no. 4, pp. 920-932, Aug. 2017.

[27] K. Kamardin, M. K. A. Rahim, P. S. Hall, N. A. Samsuri, T. A. Latef, and M. H. Ullah, "Planar textile antennas with artificial magnetic conductor for body-centric communications," *Appl. Phys. A, Mater. Sci. Process.,* vol. 122, no. 4, p. 363, 2016.

[28] S. Zhu and R. Langley, "Dual-band wearable textile antenna on an EBG substrate," *IEEE Trans. Antennas Propag.,* vol. 57, no. 4, pp. 926-935, Apr. 2009.

[29] S. Agneessens and H. Rogier, "Compact half diamond dual-band textile HMSIW on-body antenna," *IEEE Trans. Antennas Propag.,* vol. 62, no. 5, pp. 2374-2381, May 2014.

[30] H. T. Chattha, "4-Port 2-element MIMO antenna for 5g portable applications," *IEEE Access,* vol. 7, pp. 96516-96520, 2019.

[31] H. Li, S. Sun, B. Wang and F. Wu, "Design of compact single-layer textile MIMO antenna for wearable applications," *IEEE Trans. Antennas Propag.,* vol. 66, no. 6, pp. 3136-3141, June 2018.

[32] J. Deng, J. Li, L. Zhao and L. Guo, "A dual-band inverted-F MIMO antenna with enhanced isolation for WLAN applications," *IEEE Antennas and Wireless Propag Lett.,* vol. 16, pp. 2270-2273, 2017.

[33] X. Lai, Z. Xie, Q. Xie and X. Cen, "A dual circularly polarized RFID reader antenna with wideband isolation," *IEEE Antennas and Wireless Propag Lett.,* vol. 12, pp. 1630-1633, 2013.

[34] C. DS and S. S. Karthikeyan, "A novel broadband dual circularly polarized microstrip-fed monopole antenna," *IEEE Trans. Ant. Propag.,* vol. 65, no. 3, pp. 1410-1415, March 2017.

[35] J. Nocedal and S. Wright, *Numerical Optimization*, 2nd edition, Springer, New York, 2006.

UBAID ULLAH received the M.Sc and PhD degree in electrical and electronic engineering from the Universiti Sains Malaysia, in 2013 and 2017, respectively. During his PhD, he was awarded the prestigious global fellowship and the outstanding student award. He was with Engineering Optimization & Modeling Center, School of Science and Engineering, Reykjavik University, Iceland from late 2017 to early 2019. He is currently affiliated with Al Ain University, Abu Dhabi, United Arab Emirates. His research interest includes antenna theory, small antennas, antenna polarization, dielectric resonators, waveguides, millimeter-wave antenna designs, multiple-input multiple-output (MIMO) antenna system, EM-simulation-driven design, numerical analysis, microwave circuit design and optimization.

SLAWOMIR KOZIEL received the M.Sc. and Ph.D. degrees in electronic engineering from the Gdansk University of Technology, Poland, in 1995 and 2000, respectively, the M.Sc. degree in theoretical physics and the M.Sc. and Ph.D. degrees in mathematics from the University of Gdansk, Poland, in 2000, 2002, and 2003, respectively. He is currently a Professor with the School of Science and Engineering, Reykjavík University, Iceland. His research interests include CAD and modeling of microwave and antenna structures, simulation-driven design, surrogate-based optimization, space mapping, circuit theory, analog signal processing, evolutionary computation, and numerical analysis.

ISMAIL BEN MABROUK received the B.A.Sc. and M.A.Sc. degrees in electrical engineering from the University of Lille, Lille, France in 2006 and 2007, respectively and the PhD in Electrical Engineering from University of Quebec, Canada, in 2012. From 2007 to 2009 he was with Huawei Technologies, Paris, France. In 2012, he joined the Wireless Devices and Systems (WiDeS) group at University of Southern California, Los Angeles, USA. He is currently an Assistant Professor at Al Ain University of Science and Technology, Abu Dhabi, UAE. His research activities have been centred on

propagation studies for Multiple-Input and Multiple-Output (MIMO) systems, measurement campaigns in special environments, WBAN, and antenna design at the millimiter-wave and THz frequencies.